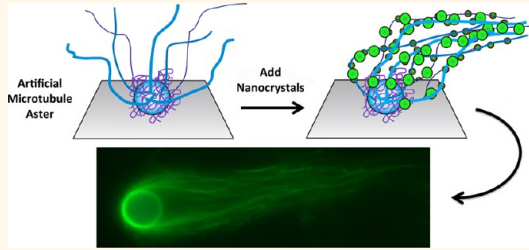


Templated Nanocrystal Assembly on Biodynamic Artificial Microtubule Asters

Erik D. Spoerke,^{†,*} Andrew K. Boal,^{‡,II} George D. Bachand,^{§,†} and Bruce C. Bunker^{†,†}

[†]Electronic, Optical, and Nano Materials, Sandia National Laboratories, Albuquerque, New Mexico, United States, [‡]Biological Interfaces and Systems, Sandia National Laboratories, Albuquerque, New Mexico, United States, [§]Nanosystems Synthesis and Analysis, Sandia National Laboratories, Albuquerque, New Mexico, United States, and [†]Center for Integrated Nanotechnologies, Albuquerque, New Mexico, United States. ^{II}Present address: MIOX Corporation, Albuquerque, New Mexico, United States.

ABSTRACT Microtubules (MTs) and the MT-associated proteins (MAPs) are critical cooperative agents involved in complex nanoassembly processes in biological systems. These biological materials and processes serve as important inspiration in developing new strategies for the assembly of synthetic nanomaterials in emerging technologies. Here, we explore a dynamic biofabrication process, modeled after the form and function of natural aster-like MT assemblies such as centrosomes. Specifically, we exploit the cooperative assembly of MTs and MAPs to form artificial microtubule asters and demonstrate that (1) these three-dimensional biomimetic microtubule asters can be controllably, reversibly assembled and (2) they serve as unique, dynamic biotemplates for the organization of secondary nanomaterials. We describe the MAP-mediated assembly and growth of functionalized MTs onto synthetic particles, the dynamic character of the assembled asters, and the application of these structures as templates for three-dimensional nanocrystal organization across multiple length scales. This biomediated nanomaterials assembly strategy illuminates a promising new pathway toward next-generation nanocomposite development.



KEYWORDS: microtubule · microtubule-associated proteins · dynamic assembly · aster · microtubule organizing center · nanocrystals · quantum dot

Nanoscale materials assembly and organization, particularly across multiple length scales and in three dimensions, remain critical challenges to the practical integration and application of nanomaterials. In the present work, we employ a bioinspired approach to templating the reversible assembly of nanocrystals in three dimensions, assembling the nanocrystals on unique artificial microtubule asters (AMAs). Our particular inspiration centers around the use of microtubules (MTs), which living organisms use as programmable nanofibers to routinely assemble, configure, and organize nanoscale building blocks into complex multifunctional materials. Assembled from α - and β -tubulin dimers, MTs are hollow protein filaments, approximately 25 nm in diameter and micrometers in length, that, along with intermediate and actin filaments, compose the cytoskeleton of eukaryotic cells.¹ Within a cell, these filaments are carefully organized and assembled as nonequilibrium architectures that can undergo controlled, reversible polymerization, a process known as dynamic instability,^{1,2} which allows assembled MT architectures to adapt in response to a cell's changing

needs. These dynamic MT filaments facilitate cellular functions including cytoskeletal restructuring, organelle positioning, separation of genetic material during cell division, and directing motor protein-based cargo transport within a cell.^{1,3,4}

The three-dimensional organization, assembly, and configuration of MTs within a cell are critical to enabling these diverse functions. One particularly intriguing example of MT organization is the microtubule aster, exemplified by the centrosome in animal cells.^{1,5,6} During the intricate and complex process of cell division, MTs carefully organized around centrosomes undergo controlled, reversible assembly and dynamic restructuring to critically facilitate precise organelle positioning, intracellular cargo transport, and chromosome separation. Inspired by the functional sophistication and precision of these dynamic, organized biological asters, we explore here artificial mimics of these structures as unique hybrid architectures and as tunable, programmable templates for synthetic nanomaterial assembly. In attempting to artificially mimic these natural materials as synthetic templates, it is

* Address correspondence to edspoer@sandia.gov.

Received for review August 30, 2012 and accepted January 30, 2013.

Published online January 30, 2013
10.1021/nn303998k

© 2013 American Chemical Society

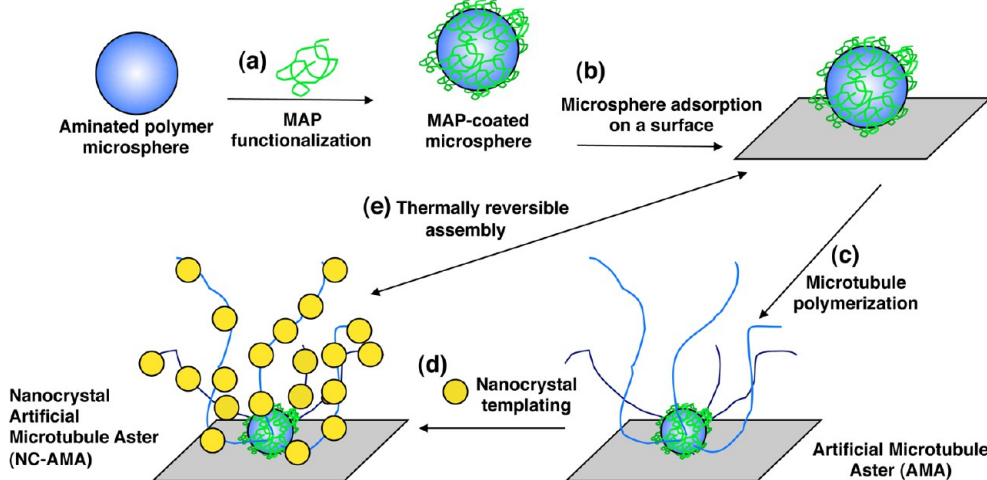


Figure 1. Illustration depicting the process of templating nanocrystals on dynamic three-dimensional microtubule asters. (a) Aminated polymer microspheres are functionalized with MAPs and adsorbed onto a glass surface (b). (c) Biotinylated MTs are polymerized onto the MAP-coated microspheres to produce biotinylated AMAs. AMAs serve as three-dimensional templates for streptavidin–QD assembly (d), which can be thermally disassembled and reassembled (e).

useful to consider the biological asters as the product of integrating four key elements: (1) MT organizing center, (2) MT filaments, (3) MT-associated proteins (MAPs),^{7–10} and (4) nanomaterial cargo to be organized, manipulated, or assembled by the centrosome aster construct. The MT organizing center itself consists of a central protein particle on which the MT filaments are nucleated, polymerized, and assembled. MAPs facilitate MT assembly and function around the organizing center by controlling MT nucleation and polymerization, regulating MT dynamic instability, and governing MT interactions with other cellular machinery. These assembled aster constructs are powerful tools for the manipulation and assembly of target nanomaterial cargo. In this paper, we illustrate how the deliberate incorporation of these elements in an artificial system can be used to create dynamic, templated, three-dimensional nanocomposites.

Creating an artificial MT aster that retains the natural biochemical and dynamic character of the MTs is a critical prerequisite to templating the reversible assembly of nanocrystals on these unique architectures. There have been a number of previous reports of different approaches to creating synthetic asters *in vitro*. These efforts have involved microtubule nucleation on isolated centrosomes^{4,11} or growing MTs from randomly oriented microtubule seeds covalently bound to micrometer-sized spheres.¹² Others have employed modified kinesin motor protein constructs that arrange preformed MTs to form densely packed asters.¹³ We have previously shown the assembly of preformed, functionally segmented MTs on functionalized microspheres to form asters with polar orientation of the radially assembled MTs.¹⁴ The use of MAPs, however, integral to MT assembly and organization *in vivo*, has not been previously explored as a means to mediate the *in vitro* assembly of MT asters as we describe here.

Our novel, MAP-based approach to AMA assembly focuses on using “structural” MAPs, such as MAP2 and

Tau protein, that are known to bind to lateral surfaces of the MTs, serving to stabilize MTs, increase MT rigidity and bundling, and even promote MT polymerization.^{1,8,9,15–17} These MAPs are relatively unstructured proteins, but contain MT-binding domains comprising three to four homologous tandem repeat sequences near the carboxy-terminus of each protein.^{8,9,15,18,19} Rich in basic residues, these binding domains attach the MAPs to the external lateral surfaces of the MTs, ostensibly *via* the acidic carboxy-termini of both α - and β -tubulin.^{9,18,20} Opposite the binding domain, the amino termini of these MAPs, relatively rich in acidic residues, project outward from the MTs, directing MT interactions with other intracellular elements.^{8,9} Such structural MAPs are especially well-suited to the assembly of AMAs, as their natural functions relate to the assembly and organization of MTs, and they can achieve these effects without unnaturally altering the intrinsic properties and behaviors of the MTs themselves. We take advantage of the biochemistry and MT-binding affinity of these MAPs as key elements that enable the reversible assembly of AMA and AMA-templated nanocomposites. As shown schematically in Figure 1, synthetic microspheres are functionalized with a commercially available mixture of MAPs, rich in MAP2 and Tau protein. These microsphere-bound MAPs then promote the capture, polymerization, and stabilization of biotinylated (or fluorescent) MTs around the synthetic microspheres to form three-dimensional artificial microtubule asters. Once formed, these biotinylated asters serve as dynamic templates, organizing streptavidin-functionalized nanocrystals to form unique three-dimensional nanocomposite architectures that can undergo biomediated reversible assembly.

RESULTS AND DISCUSSION

Although the exact mechanism of MAP functionalization on the microspheres is not yet clear, it is believed

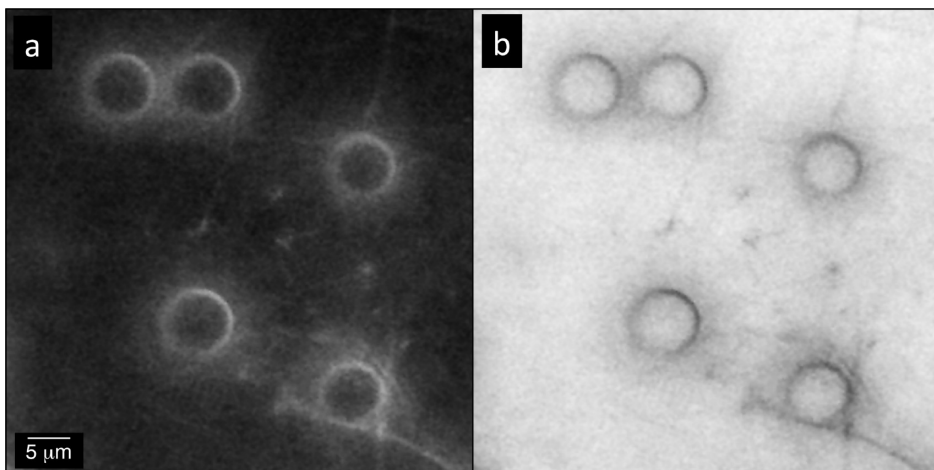


Figure 2. (a) Fluorescence micrograph of rhodamine-labeled MTs sporadically bound to aminated microspheres. For improved visual clarity, a contrast-inverted version of the image (b) is also shown. Dark lines in this inverted image show MTs associated with the microspheres.

that MAPs were functionalized onto $\sim 7 \mu\text{m}$ aminated microspheres by a combination of electrostatic attraction and covalent cross-linking. A brief pretreatment of the commercial aminated microspheres partially functionalized the beads with glutaraldehyde. A ninhydrin test for free amines²¹ determined that >90% of the amine reactivity on the beads was typically retained after the brief glutaraldehyde exposure, indicating that while some cross-linking capability was introduced to the microspheres, they retained a significant fraction of their amine functionality. During subsequent exposure to a solution of MAPs, the MAPs were bound to the microspheres, likely through electrostatic attraction between the amines on the beads and the relatively acidic projection domains of the MAPs. Glutaraldehyde cross-linking between the microsphere and lysines in the projection domains (or central portions) of the proteins provided covalent stabilization of the MAP binding.^{18,19} In this arrangement, the base-rich MT binding domains would be displayed outward on the microsphere surfaces, where they could facilitate MT capture and organization around the microspheres.

Arguably the best evidence for the successful binding of MAPs in a *functional* conformation around the microspheres is the preferential formation of MT asters around the MAP-coated beads. Figure 2 shows that rhodamine-labeled MTs polymerized in the presence of amine microspheres NOT coated with MAPs produced sporadic association of a few MTs with the beads, likely through nonspecific binding and electrostatic interactions between the positively charged beads and the negatively charged MTs. In contrast, Figure 3 shows a series of fluorescence micrographs of AMAs produced when rhodamine-labeled tubulin was polymerized in the presence of the MAP-functionalized particles. Figure 3a displays AMAs grown with fluorescent MTs extending radially from the central particles. It is worth noting that beads coated with MAPs, but not pretreated with glutaraldehyde, typically formed structures similar to those

seen in Figure 3 (see Figure 1 in the Supporting Information), although the covalent stabilization qualitatively promoted slightly higher MT densities on the beads.

The AMAs formed in the presence of MAP-coated beads also exhibited three-dimensional character, revealed in Figure 3b and c. Figure 3b shows a higher magnification image of one of the AMAs from Figure 2a, where the focus is near the AMA equator, while the image in Figure 3c was taken at the “bottom” of the an AMA, near the AMA–glass interface. In each case, MTs are clearly seen extending outward from the central particle, confirming that MTs grew over the entire 3D particle surface. Since it is known that these MAPs interact primarily with the sides of MTs,^{9,20} it is expected that these asters were formed from the growth of small segments of MTs nucleated, stabilized, and bound laterally to the bead surfaces by MAPs. A combination of crowding from densely bound MTs, MT rigidity, and bead curvature led to the extension of growing MTs outward from the central particles, producing the observed three-dimensional asters.

The overall size of the AMAs, determined by the length of the polymerized MTs, was also controllable. Figure 4 shows that by controlling the time (5–30 min) growing microtubules were allowed to polymerize at 37 °C in BRB80P, the size of the AMAs could be tuned. The inset plot in Figure 4 quantifies what is evident from the micrographs, showing that as the MT polymerization time was increased, the radii of the asters increased at a rate of $\sim 1.5 \mu\text{m}/\text{min}$, a value consistent with expected rates for MT elongation.^{1,2} The ability to tune the size of the AMAs represents a unique aspect of AMAs as biomeditated self-assembled structures and templates. Unlike systems in which preformed materials may be assembled into secondary structures, because the AMAs are *grown* as three-dimensional structures, the size of these biosynthetic architectures can be directly controlled during assembly.

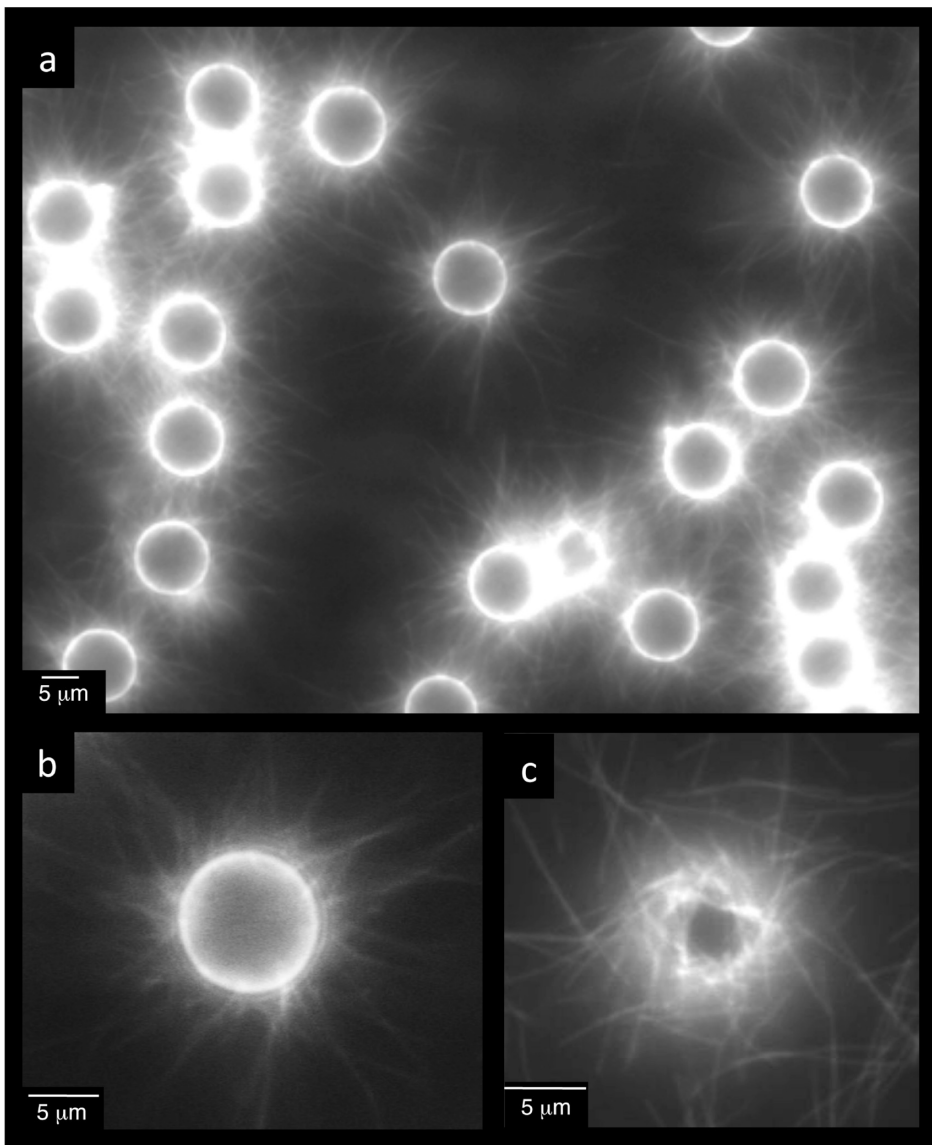


Figure 3. Fluorescence micrographs of rhodamine-labeled AMAs grown on aminated polymer beads functionalized with MAPs. (a) AMAs assembled on a glass slide showing the radial extension of MTs around the microspheres; (b) an AMA imaged near the bead equator; (c) an AMA imaged near the interface of the bead and the glass substrate.

Not only does the integration of MAPs and MTs enable the formation of unique MT asters, but the chemically functional character of these protein building blocks used makes these AMAs attractive as templates for secondary materials assembly. MTs have been previously explored as templates for growth materials such as silver²² or mineral nanowires.²³ In these examples, however, the functional character of the MTs was destroyed during material templating, making reversible assembly of these structures impossible, and the MTs templates were never assembled as complex architectures (such as the asters presented here). Here, we utilize an alternative approach, taking advantage of noncovalent biotin–streptavidin^{24,25} chemistry to selectively assemble nanocrystals (quantum dots) on the AMA templates without destroying the functional character or the MTs.^{26–28} Specifically, AMAs made using biotinylated MTs captured streptavidin-

coated quantum dots, the assembled MTs capturing and organizing these brightly fluorescent nanocrystals to form the unique three-dimensional nanocomposites. These nanocrystal–artificial microtubule asters (NC-AMAs) are shown in Figure 5.

Figure 5a and b show green fluorescent quantum dots templated on AMAs grown for short and long polymerization times, respectively. These figures clearly show how tuning the length of the MTs can be used to control the size of the AMA template and, ultimately, the size of the assembled NC-AMAs. Interestingly, these images also show how the morphology of the NC-AMAs can be varied, producing either relatively spherical asters or elongated “comet”-like structures. These comet structures are created when long MTs, grown on MAP-coated microspheres, are swept back and aligned by fluidic shear forces (generated

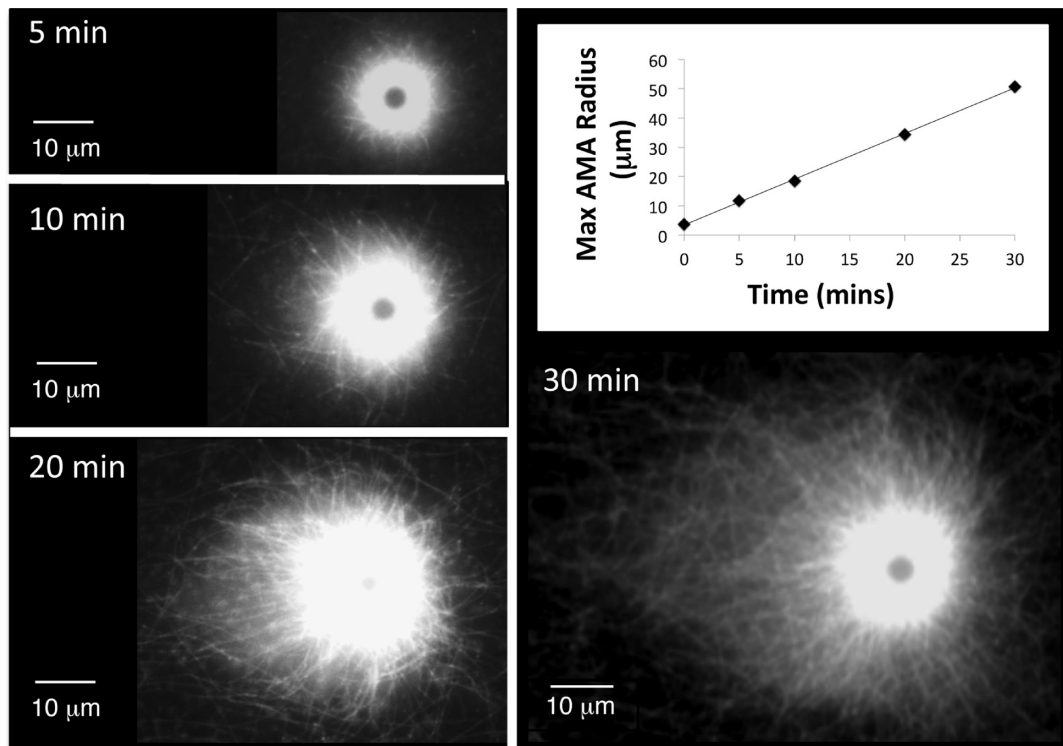


Figure 4. Fluorescent micrographs of AMAs grown for 5, 10, 20, and 30 min. Increasing growth time increased MT length, expanding the size of the overall aster. The inset plot shows a consistent MT elongation rate of $\sim 1.5 \mu\text{m}/\text{min}$.

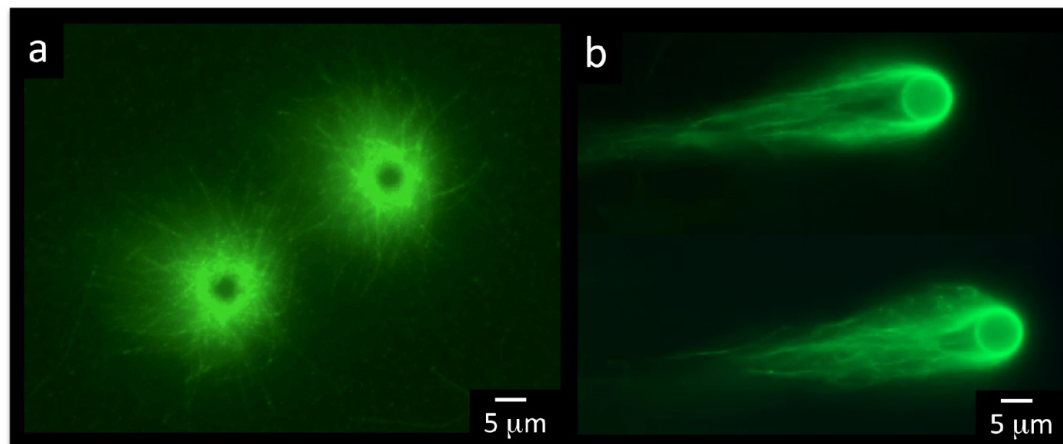


Figure 5. Fluorescent micrographs of fluorescent nanocrystals templated on microtubule asters (NC-AMAs): (a) radial NC-AMAs grown for 10 min on $\sim 7 \mu\text{m}$ MAP-coated microspheres; (b) comet-shaped NC-AMAs formed using fluid shear to orient MTs around $\sim 7 \mu\text{m}$ MAP-coated microspheres (growth time 30 min).

during fluid exchange) in the flow cells used to make the AMAs. As the biotinylated MTs come together at a comet's tail, they become linked together by the streptavidin-functionalized nanocrystals (which are each decorated with multiple streptavidin molecules), gluing these structures into their unusual form. In this instance, not only are the AMAs templating the organization and assembly of the fluorescent nanocrystals, but the nanocrystals are reciprocally serving to direct the organization of the MTs in the NC-AMAs. Using this demonstration as a model, it is easy to imagine how more complex control over fluidic shear forces could be used to produce

alternative structures as well. It is important to note that this templating process represents directed assembly of the fluorescent nanocrystals across multiple length scales. The MT templates themselves are only $\sim 25 \text{ nm}$ in diameter, but they are tens of micrometers in length. This convergence of the nanoscale and microscale in these MT templates allows for nanoscale resolution in the organization of the templated nanocrystals, extended over multiple micrometers in length.

Because biologically relevant MAPs were used to assemble the AMAs, and because nondestructive

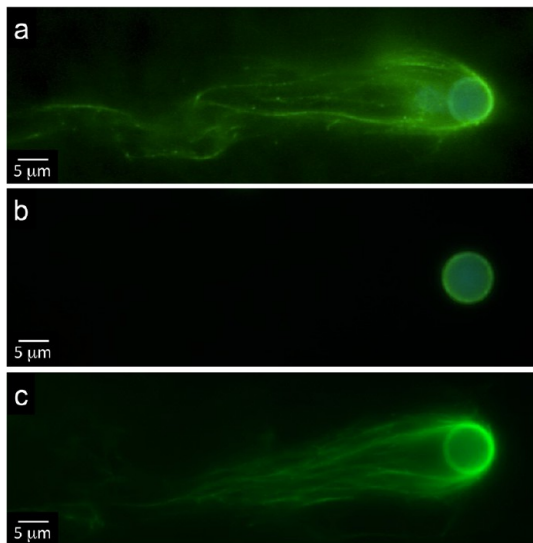


Figure 6. Fluorescence micrographs showing the thermal cycling of the NC-AMA assembly. (a) NC-AMA on a $\sim 7\text{ }\mu\text{m}$ MAP-coated microsphere as made. (b) NC-AMA after incubating at $4\text{ }^\circ\text{C}$ for 20 min. The NC-laden MTs have thermally depolymerized and been washed away. (c) NC-AMA reconstituted from a thermally depolymerized NC-AMA as in (b).

biotin–streptavidin linkages were used to assemble the nanocrystals to form the NC-AMA, the intrinsic biochemical properties of the MT building blocks were preserved in the NC-AMA composites. In particular, the nonequilibrium character of the MT supramolecular structure, critical to natural polymerization/depolymerization, could be exploited to control the reversible *in vitro* assembly and disassembly of these biocomposite nanostructures. *In vitro*, MTs can be depolymerized by a number of factors, including temperature. For example, even the Taxol-stabilized MTs used here will depolymerize below $\sim 10\text{ }^\circ\text{C}$.^{29,30} The image series in Figure 6 shows an NC-AMA comet undergoing thermally reversible assembly. This image shows that the NC comet as synthesized (Figure 6a) can be completely disassembled after cooling to $4\text{ }^\circ\text{C}$ (Figure 6b) because the MTs that make up the NC-AMA depolymerized. Because the cooling process does not degrade the MT-organizing MAPs bound to the microspheres, however, AMA formation can be recycled. Introduction of fresh reagents to the MAP-coated microspheres and reheat-*ing* to $37\text{ }^\circ\text{C}$ resulted in the re-creation of the AMAs, and addition of quantum dots as described above completely reproduced the NC-AMA structure as seen in Figure 6c. Similar thermal cyclability was observed using untemplated AMAs (no nanocrystals) as well.

Interestingly, other processes that promote MT depolymerization *in vitro*, such as elevated heating or introducing excesses of divalent cations such as Ca^{2+} , produced uncyclable disassembly of the MT templates, ostensibly because of degradation of the MAPs or cationic interference with MAP-MT binding. Nevertheless, the demonstrated thermally programmable cycling of the templated nanocomposite structures described here is uniquely enabled by the biological function of the MT templates and represents a differentiating aspect of these unusual biomediated constructs.

This biomimetic approach to nanomaterial organization and assembly stands to impact a wide range of material-based technologies. The assembly of semiconducting nanocrystals along nanoscale MT templates, organized three-dimensionally around a synthetic target, presents potential opportunities for high-rate photocatalysis or optoelectronic applications such as photovoltaics. The environmentally programmable disassembly of these fluorescent assemblies may also have implications for chemical or environmental sensing. These structures may even inform the development of new camouflage technology based on synthetic analogues to biological color changing machinery, such as that found in melanocytes, which rely on the dynamic concentration and dispersion of pigment around cellular asters to vary an organism's appearance. The continued exploration of these bioinspired, biomediated materials assemblies and processes offers great promise for next-generation materials development.

CONCLUSIONS

In summary, we have described the cooperative application of microtubules and MAPs to form three-dimensional biomimetic aster templates whose size and morphology can be controlled by regulating microtubule polymerization. Using nondestructive chemistries, we demonstrated the templating of fluorescent nanocrystals onto these templates to create novel three-dimensional nanocomposite architectures. Finally, we showed that the retained biodynamic character of the MTs used to produce these templated assemblies could be exploited to programmably assemble and disassemble these uniquely bioenabled nanocomposites. This bioinspired and biomediated approach to nanomaterials assembly represents a promising new approach to addressing the growing challenges of nanoscale materials organization and assembly.

METHODS

Tetramethylrhodamine-labeled tubulin, biotin-labeled tubulin, and microtubule-associated proteins, purified from bovine brain, were purchased from Cytoskeleton Inc. and used according to the supplier's instructions. MAPs were used as a mixed fraction

of MAP1, MAP2, and Tau isoforms, with MAP2 representing $\sim 70\%$ of the total protein content. Amine-functionalized polymer microspheres ($\sim 7\text{ }\mu\text{m}$, cat. #: PA06N) were purchased from Bangs Laboratories (Fishers, IN, USA). Streptavidin-labeled quantum dots were purchased from Invitrogen. All other reagents were purchased and used as received from common commercial sources.

Fluorescence microscopy was performed on Olympus IX71 inverted and Olympus BX51 upright microscopes using 100 \times oil immersion objectives. Black and white images were recorded using a Hamamatsu C4742-98 digital camera, while color images were obtained using a Hamamatsu C7780 3CCD digital camera.

Creating MAP-Coated Particles. A 20 μ L amount of \sim 7 μ m aminated-functionalized polymer beads was combined with 80 μ L of a 100 mM aqueous glutaraldehyde solution, which was shaken for 30 min at room temperature. The sample was centrifuged to collect the beads, and the supernatant was removed. The beads were resuspended with vortexing in 100 μ L of BRB80 (80 mM PIPES, 1 mM MgCl₂, 1 mM EGTA, pH 6.9) and recentrifuged. The supernatant was again removed, and the beads were resuspended in 20 μ L of BRB80. A 2 μ L sample of this solution was added to 25 μ L of a 1 mg/mL MAP solution in MAP buffer (10 mM piperazinebis(ethanesulfonic acid) (PIPES), 0.3 mM ethylene glycol bis(β -aminoethyl ether-*N,N,N',N'*-tetraacetic acid (EGTA), and 3% (w/v) sucrose, pH 7.5), which was then shaken for 30 min at room temperature, and the resulting suspension used without purification.

Growth of Artificial Microtubule Asters. AMAs were grown both as suspended particles and within coverslip flow cells, using identical processing, although rinses for the suspended particles were achieved using centrifugation. Although both were effective, AMAs grown on coverslips were more readily imaged and are the focus of this work. Coverslip flow cells were assembled by first placing two pieces of double-sided transparent tape (0.1 mm thick), each \sim 3–4 cm long, aligned parallel to one another and spaced approximately 6–7 mm apart, onto a large glass coverslip (24 mm \times 50 mm). A second coverslip (25 mm \times 25 mm) was placed over the tape strips, creating a channel with a volume slightly less than 20 μ L between the pieces of tape, sealed above and below by the glass coverslips. A 20 μ L aliquot of the MAP-functionalized bead suspension was pipetted into one end of this channel and incubated for 5 min at room temperature to allow some of the beads to adhere to the glass surface. The cell was then washed twice with 20 μ L aliquots of BRB80 flowed through the cell before introducing a 1 mg/mL solution of rhodamine tubulin in BRB80P (BRB80 + 1 mM guanosine triphosphate and 10% glycerol) into the cell. The sample was then incubated for 5–30 min on an aluminum block heated to 37 °C. The cell was then rinsed twice with 20 μ L aliquots of BRB80T (BRB80 + 2 μ m Taxol), which had been warmed to 37 °C. A final aliquot of BRB80TAF (BRB80T containing an antifade mixture of 1 μ L of 2 M dextrose, 1 μ L of 100 mM magnesium adenosine triphosphate, 1 μ L of 0.8 mg/mL catalase, 1 μ L of 2 mg/mL glucose oxidase, and 0.5 μ L of 2-mercaptoethanol) was flowed through the cell prior to fluorescence imaging.

Templated Assembly of Nanocrystal AMAs. AMAs were grown as above, using tubulin growth solutions containing a 1:4 mixture of biotinylated and unlabeled tubulin. Once stabilized with BRB80T, a solution containing streptavidin-coated quantum dot nanocrystals diluted 10 \times in BRB80T was flowed into the cell. The cell was incubated for 1 min at room temperature and then washed twice with BRB80T, followed by fluorescence imaging under UV excitation.

Reversible Growth of AMAs and NC-AMAs. AMAs and NC-AMAs were grown as described above and checked by fluorescence microscopy. The flow cell containing the AMAs in BRB80T was then incubated at 4 °C for 90 min. The flow cell was then washed twice with BRB80T and once with BRB80TAF and imaged under the microscope. This cell was then flushed twice with BRB80P, followed by the addition of a 20 μ L aliquot of a 1 mg/mL solution of tubulin (rhodamine-labeled or biotinylated as described above) in BRB80P, and heated to 37 °C for 20 min. The cell was then rinsed with two 20 μ L aliquots of BRB80T (prewarmed to 37 °C) and one 20 μ L aliquot of BRB80TAF before imaging by fluorescence microscopy.

Conflict of Interest: The authors declare no competing financial interest.

Supporting Information Available: A fluorescence micrograph of MT asters formed around beads noncovalently functionalized with MAPs is available free of charge via the Internet at <http://pubs.acs.org>.

Acknowledgment. This work was supported by the U.S. Department of Energy, Office of Basic Energy Sciences, Division

of Materials Sciences and Engineering. Sandia National Laboratories is a multiprogram laboratory managed and operated by Sandia Corporation, a wholly owned subsidiary of Lockheed Martin Corporation, for the U.S. Department of Energy's National Nuclear Security Administration under contract DE-AC04-94AL85000.

REFERENCES AND NOTES

1. Lodish, H.; Berk, A.; Zipursky, S.; Matsudaira, P.; Baltimore, D.; Darnell, J. *Cell Motility and Shape II: Microtubules and Intermediate Filaments*. In *Molecular Cell Biology*, 4th ed.; W.H. Freeman and Co.: New York, NY, 2000; pp 795–847.
2. Fygenson, D.; Braun, E.; Libchaber, A. Phase Diagram of Microtubules. *Phys. Rev. E* **1994**, *50*, 1579–1588.
3. Mitchison, T.; Kirschner, M. Dynamic Instability of Microtubule Growth. *Nature* **1984**, *312*, 237–242.
4. Schnackenberg, B.; Khodjakov, A.; Rieder, C.; Palazzo, R. The Disassembly and Reassembly of Functional Centrosomes *In Vitro*. *Proc. Natl. Acad. Sci. U. S. A.* **1998**, *95*, 9295–9300.
5. Brinkley, B. Microtubule Organizing Centers. *Annu. Rev. Cell Biol.* **1985**, *1*, 145–172.
6. Bornens, M. The Centrosome in Cells and Organisms. *Science* **2012**, *335*, 422–426.
7. Bonnett, C.; Boucher, D.; Lazereg, S.; Pedrotti, B.; Islam, K.; Denoulet, P.; Larcher, J. Differential Binding Regulation of Microtubule-Associated Proteins Map1a, Map1b, and Map2 by Tubulin Polyglutamylation. *J. Biol. Chem.* **2001**, *276*, 12839–12848.
8. Dehmelt, L.; Halpain, S. The Map2/Tau Family of Microtubule-Associated Proteins. *Genome Biol.* **2004**, *6*, 204.1–204.9.
9. Goedert, M.; Crowther, R.; Garner, C. Molecular Characterization of Microtubule-Associated Proteins Tau and Map2. *Trends Neurosci.* **1991**, *14*, 193–199.
10. Halpain, S.; Dehmelt, L. The Map1 Family of Microtubule-Associated Proteins. *Genome Biol.* **2006**, *7*, 224.1–224.7.
11. Stearns, T.; Kirschner, M. *In Vitro* Reconstitution of Centrosome Assembly and Function: The Central Role of Gamma-Tubulin. *Cell* **1994**, *76*, 623–637.
12. Holy, T.; Dogterom, M.; Yurke, B.; Leibler, S. Assembly and Positioning of Microtubule Asters in Microfabricated Chambers. *Proc. Natl. Acad. Sci. U. S. A.* **1997**, *94*, 6228–6231.
13. Nedelec, F.; Surrey, T.; Maggs, A.; Leibler, S. Self-Organization of Microtubules and Motors. *Nature* **1997**, *389*, 305–308.
14. Spoerke, E.; Bachand, G.; Liu, J.; Sasaki, D.; Bunker, B. Directing the Polar Organization of Microtubules. *Langmuir* **2008**, *24*, 7039–7043.
15. Aizawa, H.; Emori, Y.; Murofushi, H.; Kawasaki, H.; Sakai, H.; Suzuki, K. Molecular Cloning of a Ubiquitously Distributed Microtubule-Associated Protein with Mr 190,000. *J. Biol. Chem.* **1990**, *265*, 13849–13855.
16. Murphy, D.; Borisy, G. Association of High-Molecular-Weight Proteins with Microtubules and Their Role in Microtubule Assembly *In Vitro*. *Proc. Natl. Acad. Sci. U. S. A.* **1975**, *72*, 3696–2700.
17. Murphy, D.; Johnson, K.; Borisy, G. Role of Tubulin-Associated Proteins in Microtubule Nucleation and Elongation. *J. Mol. Biol.* **1977**, *117*, 33–52.
18. Lewis, S.; Wang, D.; Cowan, N. Microtubule-Associated Protein Map2 Shares a Microtubule Binding Motif with Tau Protein. *Science* **1988**, *242*, 936–939.
19. Lee, G.; Cowan, N.; Kirschner, M. The Primary Structure and Heterogeneity of Tau Protein from Mouse Brain. *Science* **1988**, *139*, 285–288.
20. Kim, H.; Binder, L.; Rosenbaum, The Periodic Association of Map2 with Brain Microtubules *In Vitro*. *J. Cell. Biol.* **1979**, *80*, 266–276.
21. Sarin, V.; Kim, Y.; Fox, J. Quantitative Monitoring of Solid-Phase Peptide Synthesis by the Ninhydrin Reaction. *Anal. Biochem.* **1981**, *117*, 147–157.
22. Behrens, S.; Wu, J.; Habicht, W.; Unger, E. Silver Nanoparticle and Nanowire Formation Nby Microtubule Templates. *Chem. Mater.* **2004**, *16*, 3085–3090.

23. Boal, A.; Headley, T.; Tissot, R.; Bunker, B. Microtubule-Templated Biomimetic Mineralization of Lepidocrocite. *Adv. Funct. Mater.* **2004**, *14*, 19–24.
24. Moy, V.; Florin, E.-L.; gaub, H. Intermolecular Forces and Energies between Ligands and Receptors. *Science* **1994**, *266*, 257–259.
25. Zhang, Z.; Moy, V. Cooperative Adhesion of Ligand-Receptor Bonds. *Biophys. Chem.* **2003**, *104*, 271–278.
26. Bachand, G.; Rivera, S.; Boal, A.; Gaudioso, J.; Liu, J.; Bunker, B. Assembly and Transport of Nanocrystal CdSe Quantum Dot Nanocomposites Using Microtubules and Kinesin Motor Proteins. *Nano Lett.* **2004**, *4*, 817–821.
27. Hess, H.; Vogel, V. Molecular Shuttles Based on Motor Proteins: Active Transport in Synthetic Environments. *Rev. Mol. Biotech.* **2001**, *82*, 67–85.
28. Liu, H.; Spoerke, E.; Bachand, M.; Koch, S.; Bunker, B.; Bachand, G. Biomolecular Motor-Powered Self-Assembly of Dissipative Nanocomposite Rings. *Adv. Mater.* **2008**, *20*, 4476–4481.
29. Kirschner, M.; Williams, R.; Weingarten, M.; Gerhart, J. Microtubules from Mammalian Brain: Some Properties of Their Depolymerization Products and a Proposed Mechanism of Assembly and Disassembly. *Proc. Natl. Acad. Sci. U. S. A.* **1974**, *71*, 1159–1163.
30. Melki, R.; Carlier, M.-F.; Pantaloni, D.; Timasheff, S. Cold Depolymerization of Microtubules to Double Rings: Geometric Stabilization of Assemblies. *Biochemistry* **1989**, *28*, 9143–9152.